**Proceedings of the Canadian Society for Mechanical Engineering International Congress 2021**
**CSME Congress 2021**
**June 27-30, 2021, Charlottetown, PEI, Canada**

# Dynamic overflow leakage in Archimedes screw generators

**Published as:**

Simmons S, Dellinger G, Aliabadi AA, Lubitz WD. Dynamic overflow leakage in Archimedes screw generators. In Proceedings of the Canadian Society for Mechanical Engineering International Congress 2021 CSME Congress Charlottetown PEI Canada 2021 (Vol. 1).

Scott Simmons[1], Guilhem Dellinger[2], Amir A. Aliabadi[1], William David Lubitz[1*]
[1]School of Engineering, University of Guelph, Guelph, Canada
[2]ICube Laboratory, ENGEES, Strasbourg, France
*wlubitz@uoguelph.ca

***Abstract***— The dynamic overflow leakage phenomenon has been introduced in Archimedes screw generator research, but it has not been discussed in the literature in much detail. The authors sought to examine this phenomenon in greater detail by computational fluid dynamic (CFD) studies supported with experimental observations. The CFD results indicated that surface roughness had a significant impact on frictional power losses as well as overflow leakage in Archimedes screws. The results gathered and documented in this study will aide in further performance predicting model development to optimize the design and power production of Archimedes screw generator powerplants.

***Keywords-Archimedes screw generator; hydrodynamic screw; computational fluid dynamics; microhydro generation; overflow leakage; thin film flow; efficiency; surface roughness***

## I. INTRODUCTION

Archimedes screws have been used to pump water since antiquity and have recently been used as hydro-electric generators (Fig. 1); in this latter function it is commonly called an Archimedes screw generator (ASG). The simple, robust design of ASGs has been advantageous for hydropower plants as they are easy and cost effective to manufacture, maintain, and operate, with low environmental impacts.

ASGs were shown to be less expensive options than other hydro-turbine technologies with similar operational ranges [1]. This is because screw plants are less complex systems with coarser inflow screening requirements [2] that can be retrofitted to old mill sites and flood control dams [3].

Maintenance and operating costs for ASGs are low [4]. ASGs require less routine maintenance than other turbine technologies [5]. Regular fluid level checks are required. Routine cleaning may be required for screws installed in nutrient-rich waterways that stimulate significant algal growth on the blades and inner cylinder of the screw [6]. Major refurbishment is usually planned on a 20-30 year cycle [3], [5].

Archimedes screws are widely viewed as an "eco-friendly" hydropower option. They usually operate as run-of-river systems which have been shown to have less negative environmental impacts than conventional hydropower [7]. As well, sediment, debris, and fish can pass through an operating ASG. Most literature suggests ASGs do not significantly harm fish [8]–[11], however, one study found significant injury and mortality rates [12]. Injury and mortality tend to be the result of bad practice in site design. Design guidelines suggest practices that reduce harm, for example, by removing pinch points and installing rubberized bumpers on screw flight leading edges when tip speeds pass 3.5 m/s [13]. Further, downstream fish migration did not seem to be effected by an ASG powerplant [10], [14]. Disorientation and increased predation were not found at the outlet of ASGs [9], [11], however, a recent paper noted increased presence of a predator species downstream of an installation during parts of a study [10].

Screw generators have a relatively wide operational range for a micro-hydropower technology. There have been successful implementations of screw generators at sites with a head of $h$ = 0.1 m and a flow rate of $Q$ = 0.01 m$^3$/s [15]. Larger sites have been successful with heads near 5 m [16] and flow rates of nearly 15 m$^3$/s [17]. Within these bounds, ASGs

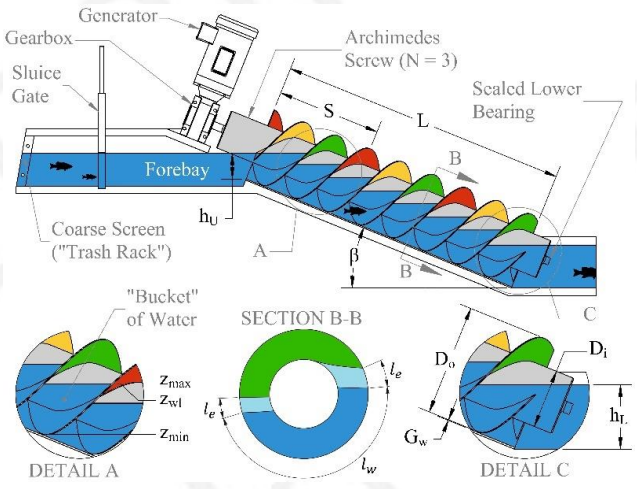


Figure 1. Archimedes screw geometry, layout, and dimensions. Detail A shows "bucket" water level variables. Section B-B shows gap leakage modelling variables. Detail C highlights the gap width and outlet water level.

usually operate between 60 % to 80 % river-to-wire efficiency [18]–[20]; however, some installations have operated at higher efficiencies [21], [22]. ASGs tend to perform at similar efficiencies to other technologies in this range of plant sizes [23].

During operation, water enters the top of the screw and begins to form a volume of water between two adjacent blades, this is often referred to as a "bucket" in the literature (cf. Fig. 1). Geometrically, the continuous helical volume that forms along the length of the screw between two adjacent flights is called a "chute" – multiple buckets usually form along one chute. Fill height ratio ($f$) can be used to quantify the water level within a bucket for modelling purposes

$$f = \frac{z_{wl} - z_{min}}{z_{max} - z_{min}} \tag{1}$$

where $z_{min}$ and $z_{max}$ (cf. Fig. 1, Detail A) are the lowest and highest water levels possible in a bucket without overflow.

Archimedes screw generators have been described as quasi-static systems since power is produced by converting the dominantly static pressure in a bucket into rotational energy [24]. The main power losses during production are related to dynamic phenomena, such as friction between water and moving surfaces, fluid effects at inlets and outlets, and water leakage from buckets.

Performance models are documented in the literature that have been used to aide design optimization of ASG powerplants. The modelling techniques used by Nuernbergk [25], [26], Lubitz et al. [20], [27], and Rohmer [28] are generally similar. Bucket water level is evaluated and used to compute the torque corresponding to static pressure differences across the blades. Loss models are applied afterwards to correct the performance predictions. However, many of the loss modules presented in the literature could be improved with a more robust range of experimental data to aide in development. Current models account for the aforementioned losses [20], [26], [29], but neglect dynamic effects when calculating gap leakage and overflow leakage. In particular, overflow leakage loss could be improved since some fluid properties of this phenomenon are not currently accounted in existing models.

The two forms of leakage in ASGs are overflow, and gap leakage. Gap leakage occurs as water passes into an adjacent bucket via the small gap (denoted $G_w$ in Fig. 1) between the blade tips and the trough. Overflow leakage ($Q_o$) occurs when water levels in a bucket are high enough to allow some water to exit the bucket by passing over the top of the inner cylinder into the next lowest bucket in the same chute; as seen specifically in Fig. 2a. This study found that there are two modes of overflow leakage; the terms "static overflow" and "dynamic overflow" will be used to describe these modes, which are discussed in detail later.

**(a)** **(b)**

Figure 2. Dynamic overflow leakage observed at (a) Buckfast Abbey and (b) Romney Weir (b).

Static overflow leakage occurs when the bucket fill height ratio exceeds unity ($f > 1$, cf. Fig. 2a). A fill height above unity indicates that water will overtop the central tube of the screw and spill into the next lowest bucket of the chute. The static overflow phenomenon is well documented in the literature [26], [27]. The most common approach to model overflow leakage focusses strictly on static overflow, and the authors refer to it as the "Aigner method" [26], [27], [30]:

$$Q_o = \frac{4}{15}\mu\sqrt{2g}\left(\frac{1}{\tan\beta} + \tan\beta\right)(z_{wl} - z_{max})^{5/2} \tag{2}$$

where $\beta$ is the screw inclination angle, $g$ is the gravitational constant, and $\mu$ is a weir-flow coefficient that is usually set to $\mu = 0.536$ [26], [31].

An adaptation to the Aigner method that includes a rotation speed term was recently proposed [29]. Conceivably, though we are referring to it as static overflow, a rotation speed term should be present to account for frictional resistance to overflow. Unfortunately, the resulting updated model was developed empirically with laboratory-scale data [29], and so it may not be broadly applicable to real-world ASG powerplants.

Dynamic overflow leakage is a function of two-phase boundary layer mechanics. A thin film develops on the blades and inner cylinder of the screw and is drawn up and into the previous bucket along a chute; this was visualized at the screw powerplant shown in Fig. 2b. As this study will demonstrate, the dynamic overflow leakage increases significantly with surface roughness.

This study investigates the factors that contribute to overflow leakage in Archimedes screw generators. The research presented in this article was conducted to improve overflow modelling techniques. The literature contains experiments and field studies; however, those studies do not contain the data necessary for more in-depth overflow leakage modelling. Generally, it is difficult to gather useful real-world data from ASGs during operation since simultaneous measurements of upper and lower water level, flow rate, torque, and rotation speed are required. Overflow modelling, also requires measurements of bucket fill height and the thin film that develops during dynamic overflow, further increasing experimental complexity.

The authors have developed a full-scale computational fluid dynamics (CFD) model that simulates ASG operation within an upper and lower basin with a dynamically meshed screw. Data from laboratory experiments and real-world ASG powerplants were collected to evaluate the CFD model. The evaluated CFD model was then used to simulate a range of surface roughness values and scale sizes of screws to lay the experimental groundwork for further overflow leakage model development.

Table I. Laboratory and real-world screw dimensions and operating parameters.

| ASG Site | Location | $D_o$ (m) | $L$ (m) | $\beta$ (°) | $N$ (-) | Rated Power (kW) | Rated Head (m) | Rated Flow ($m^3/s$) |
|---|---|---|---|---|---|---|---|---|
| *Laboratory Screw A* | Guelph, Canada | 0.150 | 0.600 | 24.9 | 3 | 0.0011 | 0.22 | 0.00107 |
| *Laboratory Screw 2* | Guelph, Canada | 0.318 | 1.22 | 24.5 | 3 | 0.058 | 0.49 | 0.01 |
| *Laboratory Screw 15* | Guelph, Canada | 0.381 | 0.617 | 24.5 | 4 | 0.034 | 0.32 | 0.014 |
| *Fletcher's Horse World* | Waterford, Canada | 1.40 | 4.50 | 22 | 3 | 7.2 | 1.7 | 0.54 |
| *Buckfast Abbey* | Buckfastleigh, UK | 2.50 | 10.5 | 26 | 4 | 84 | 4.2 | 2.8 |
| *Ruswarp Hydro* | Whitby, UK | 2.90 | 5.12 | 22 | 3 | 50 | 1.8 | 4 |
| *HydroSmart Srl Hydro* | Valpagliaro, Italy | 3.60 | 7.40 | 22 | 4 | 121 | 3.0 | 5.5 |

## II. METHODOLOGY

Data was gathered across a wide range of screw scale sizes as shown in Table I. As previously mentioned, simultaneous measurements of flow rate, up- and downstream water levels, rotation speed, and torque were required in datasets for validating ASG models.

### A. *Laboratory Experiments*

Laboratory experiments were carried out at the University of Guelph (Ontario, Canada). Measurements were all recorded digitally, then verified and documented with analogue measurements to ensure accurate datasets. The laboratory apparatus (Fig. 3) is discussed briefly in this section. Further details may be found in the literature [32].

The apparatus consisted of three water basins (the weir basin, upper basin and lower basin), an Archimedes screw, variable frequency drive (VFD) motor/generator, and instrumentation to measure and collect data during operation. The Archimedes screw was placed between the upper and lower basin. Water was pumped at a desired rate from the lower basin (the most downstream end of the system) into the weir basin (the most upstream end of the system). Flow rate was measured with a propeller-type flow meter placed within the piping between the two basins. Water upfilled in the weir basin and then passed through two parallel Cipoletti weirs into the upper basin. The water level passing over the Cipoletti weirs was measured and known weir relationships were used to estimate and verify flow meter measurements. Water then passed from the upper basin to the lower basin via the screw. Screw rotation speed was set and maintained by the VFD.

Figure 3. University of Guelph Archimedes screw apparatus.

Water level in each basin was measured with digital depth sensors set in stilling wells. Depth measurements were verified using manual measurements of water level. Rotation speed was measured with a magnetic tachometer and verified with a handheld optical unit. Finally, torque was measured with a load cell and moment arm assembly. The moment arm was mounted to the VFD, and the load cell was attached between the moment arm and a fixed point on the apparatus frame.

A dataset with more than 1500 unique data points has been gathered with this experimental setup. Details are documented in the literature; this study used data from this set [32]–[36].

### B. *Field Measurements*

Data was also gathered from four different real-world installations for this study. They will be introduced and discussed in this section in order of their scale size (i.e. from smallest to largest outer diameter).

The installation at Fletcher's Horse World in Waterford, Ontario, Canada (Fig. 4a) is rated to produce 7.2 kW and operates as a single, fixed-speed screw in a covered and air-sealed enclosure. Sealed enclosures prevent ice build-up in colder climates and algal growth in high-nutrient waterways. Flow rate was measured at the most upstream opening of the installation's inlet channel. An acoustic velocimeter (FlowTracker2® Acoustic Doppler Velocimeter®, Sontek, 2016) was used to sample water velocity in a grid pattern at the

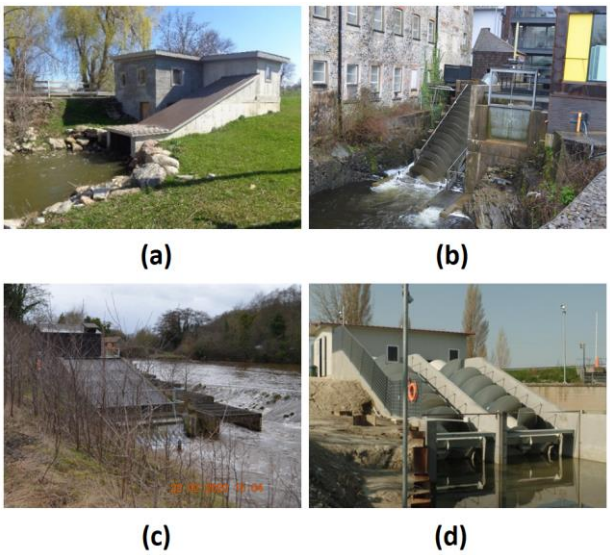


Figure 4. Real-world ASG powerplants: (a) Fletcher's Horse World, Waterford, Ontario, Canada, (b) Buckfast Abbey, Buckfastleigh, Devon, UK, (c) Ruswarp Hydro, Whitby, Yorkshire, UK, (d) HydroSmart Srl. Hydro, Valpagliaro, Ferrara, Italy.

inlet; measurements were then integrated about the grid to compute the inlet flow rate.

Up- and downstream water levels were measured with surveying equipment – requiring one individual to operate a manual transit and another to handle a surveying pole. Rotation speed was verified optically using a DSLR camera and adding a reference point on the installation frame. Torque was calculated from electrical power readings, rotation speed and gearbox data.

Similar methods were employed at the other powerplants. The Buckfast Abbey installation in Buckfastleigh, Devon, UK (Fig. 4b) is a moderate-sized, fixed-speed, single-screw installation. Flow rate was again found by integrating a grid pattern of velocity measurements made with the acoustic velocimeter. Multiple flow measurements were conducted at this site to develop a relationship between water level and flow rate within the inlet channel of the powerplant. Water level up- and downstream were measured with survey equipment to verify on-site gauge accuracy. The data collected from the gauges was then deemed accurate and used in the study. Rotation speed of the fixed-speed system was verified optically, and screw torque was again approximated by measuring electrical power and estimating system losses.

The Ruswarp ASG near Whitby, Yorkshire, UK (Fig. 4c), is a single, variable-speed screw. Flow rate was measured in a similar method as outline above, for three different inlet water levels. The sluice gate was manually adjusted at the inlet to modify the water level and flow rate entering the screw. A higher-resolution grid was measured for the first flow rate, and coarser grids for the two other inlet conditions. Channel geometry variation led to high uncertainty in the coarser measurements, so only the higher-resolution data was used from this site. Up- and downstream water level was again measured by on-site depth sensors and verified with surveying techniques. Rotation speed was recorded on-site and verified optically. Electrical power readings were gathered and used to approximate screw torque similarly to the other studies.

The HydroSmart Srl powerplant at the Lock of Valpagliaro, Ferrara, Italy (Fig. 4d) uses two large, identical, parallel screws. The site is very well instrumented; measurements and data are presented and discussed in detail in the literature [22], [37]–[39]. The site operators provided measured flow rate, up- and downstream water levels, electrical power, some power losses, and rotation speed. The authors visited the site to confirm conditions.

### C. *Numerical Simulations*

A full-scale, dynamically meshed ASG was modelled as a three-dimensional, transient, two-phase Reynolds-averaged Navier-Stokes (RANS) computational fluid dynamic (CFD) simulation. The model was initially developed at the ICube Laboratory (Strasbourg, France) using OpenFOAM 5.0 [40]. The governing equations and simulation implementation are detailed in the literature [41], [42].

New modelling, formulation, and post processing techniques were adapted through collaboration between the University of Guelph and the ICube Laboratory using OpenFOAM 4.0. Details of the basic formulation of this adapted model are available in the literature [43]. The simulation domain is shown in Fig. 5.

The CFD simulations were initialized with a volume of water in the upper and lower basins, then run for 30-seconds of simulated time. Convergence was identified as the point when the torque had reached a regularly oscillating state, termed "quasi-steady state" by the authors (Fig. 6). In this state, the volume of water entering and exiting the system has equilibrated. The oscillations in torque values are due to the filling and emptying of buckets during operation at the inlet and outlet of the screw, respectively. The authors demonstrated that the amplitude of these oscillations depend on the inclination angle of the screw; steeper screws have larger oscillations at quasi-steady state [43].

Simulations were run to match the dimensions and operating conditions of the screws shown in Table I. for the model evaluation. Afterwards, simulations were carried out for seven geometrically similar screws at a range of scales. This set of simulations was developed to allow observation of scale effects on a range of ASG phenomena. This supports development of performance models to accurately predict ASG efficiency at all useful sizes.

The authors selected Laboratory Screw 2 (cf. Table I.) as the base scale since it was the most widely tested laboratory screw. The six other scale-sized models were geometrically scaled from Screw 2 dimensions. Therefore, all CFD models had the same diameter ratio ($D_i/D_o = 0.532$), pitch-diameter ratio ($S/D_o = 1.00$), pitch-length ratio ($S/L = 0.260$), number of

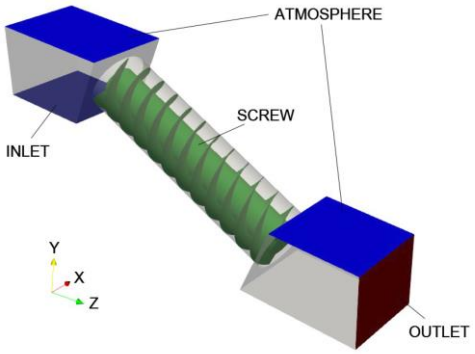


Figure 5. CFD model domain highlighting the main boundary conditions.

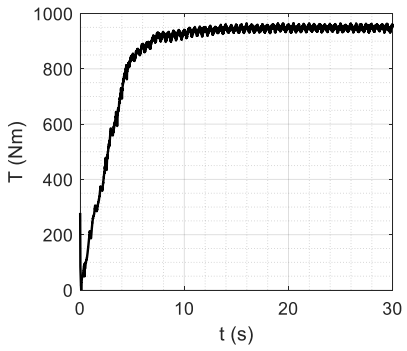


Figure 6. Convergence of simulated torque (T) over time (t).

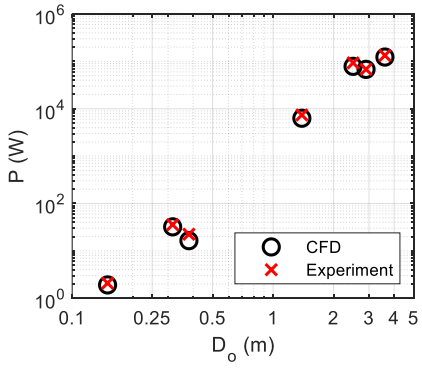


Figure 7. Comparison of CFD predictions and experimental data.

blades (N = 3), and inclination angle (β = 24.5°).

The seven scaled outer diameters are $D_o$ = 0.148 m, 0.316 m, 0.675 m, 1.00 m, 2.00 m, 3.50 m, and 5.00 m. Additionally during this study, simulations of the $D_o$ = 2 m scale-sized screw were conducted at a fill level of $f$ = 1, over a range of five different surface roughness heights $z_0$ = 0 mm, 0.3 mm, 1.0 mm, 2.4 mm, 11.4 mm, and 37.0 mm. These roughness values correspond to Gauckler-Manning coefficients of $n$ = 0, 0.010, 0.012, 0.014, 0.018, and 0.022, respectively. These values were selected since they represent the range of surface roughness values that could practically be observed in real-world installations. The highest values represent a screw with substantial algal growth on the blades and inner cylinder.

## III. Results and Discussion

### A. CFD Model Evaluation

Results of the numerical simulations were compared to the experimental data (Fig. 7). The model seemed to perform well as it predicted similar power production values compared to the experimental data. There are small differences in the results. The CFD model is a "perfect" geometrical representation of an Archimedes screw; even given a surface roughness, there are no imperfections or slight differences within the tolerable range of manufacturing that occur in a real-world screw. As such, the gap width ($G_w$, cf. Fig. 1, Detail C) may differ slightly between simulation and reality – causing some differences in gap leakage loss. Frictional losses and entrance losses may, in turn, exhibit similar differences. Further, flow rate was set to match between the experiments and simulations, so any uncertainty or error in the on-site flow measurements was propagated through the numerical simulations. Nonetheless, the comparison in Fig. 7 suggests that the CFD model successfully approximates the performance of Archimedes screw generators. Therefore, the authors suggest the model is a reasonably accurate approximation of the performance of ASGs, and it is appropriate for further analysis and model development.

### B. Dynamically Impacted Losses

The numerical simulations provided new insight into the mechanics of ASG power losses, including those related to gap leakage, friction loss, and overflow leakage.

The authors recently demonstrated that rotation speed drives the relative velocity of fluid flowing through the gap region [24], meaning gap leakage rate is affected by rotation speed. Since this region is occupied by a gap only, no blades can convert pressure to rotation. Thus, the gap region does not contribute to energy production, but leakage loss may be minimized to decrease its impact on power production. It was theorized that at very high speeds, the blades may "outrun" the gap leakage rate, and cause negative gap leakage [24]. At an intermediate point there may be an optimal operating point with regards to gap leakage.

Fig. 8 shows friction loss as a function of surface roughness in the $D_o$ = 2 m scale-screw, with all variables in non-dimensional form. Power production ($P_s$) was non-dimensionalised by the available power ($P_a$), yielding the mechanical efficiency ($\eta$):

$$\eta = \frac{P_s}{P_a} = \frac{T\omega}{\rho g h Q} \tag{3}$$

where the available power is the product of water density ($\rho$), the gravitational constant ($g$), overall head ($h$) and total flow rate ($Q$). For reference, mechanical shaft power is shown in its base terms of torque ($T$) and rotation speed ($\omega$). The frictional power loss was non-dimensionalised by the available power as well to keep the two variables in the same terms.

The Darcy-Wiesbach friction factor ($f_D$) was used to represent the surface roughness in dimensionless terms. It was computed with the Colebrook-White equation, which requires an iterative solution in terms of surface roughness ($z_0$), length-scale ($D_h$), and the Reynolds number ($Re$):

$$\frac{1}{\sqrt{f_D}} = -2\log\left(\frac{z_0}{3.7D_h} + \frac{2.51}{Re\sqrt{f_D}}\right) \tag{4}$$

In Fig. 8, surface roughness had a significant impact on power production and power loss. Intuitively, as surface roughness increased, frictional power loss increased, and overall power production dropped. Fitting a trendline to the curve suggested that frictional power loss followed a similar trend to that of a 2nd order system. This seemed like an appropriate result since friction loss is a function of area – itself

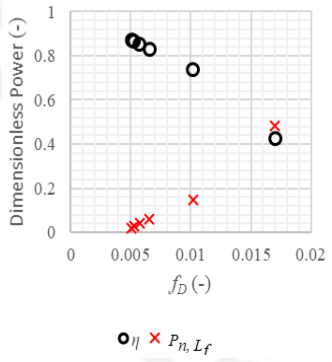


Figure 8. Dimensionless power as a function of surface roughness. Dimensionless power production is given as the mechanical efficiency ($\eta$) and frictional loss ($P_{n,Lf}$) is non-dimensionalised with a similar approach.

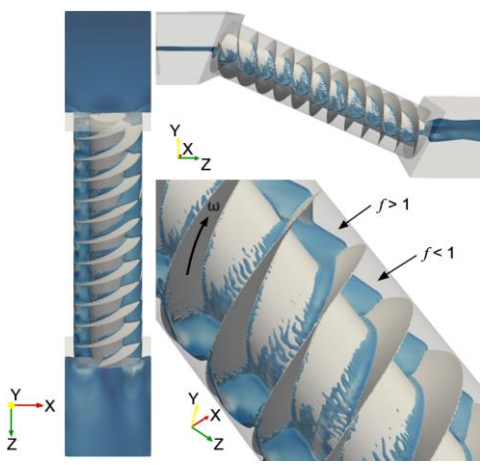


Figure 9. CFD simulation results of the $D_o$ = 2 m scale-size screw operating at $f$ = 1 with a surface roughness of $n$ = 0.014. Rotation direction is indicated on the bottom right screw blade.

the second order of a length-scale.

The changing frictional loss is expected to affect other loss modes. The literature has some discussions of a friction-leakage flow that forms by water adhering to the blades of the screw [26], [30]; but modelling of this phenomenon seems sparse. It is suggested that this frictional leakage is a dynamic form of overflow leakage – the authors have referred to it as "dynamic overflow leakage". This loss was impacted by surface roughness and is explored in further detail below.

### *C. Overflow Leakage*

As mentioned, overflow leakage has two forms, static and dynamic overflow leakage; Fig. 9 demonstrates both forms of overflow leakage. Though the ASG in Fig. 9 is operating at $f$ = 1, it still experiences static overflow leakage due to a "sloshing" phenomenon within the buckets. The bucket water levels vary along the length of the screw. This is because the water in the buckets were sloshing as it translated along the screw from inlet to outlet, due to wave formation during water inrush to the screw entrance. The sloshing caused cases of

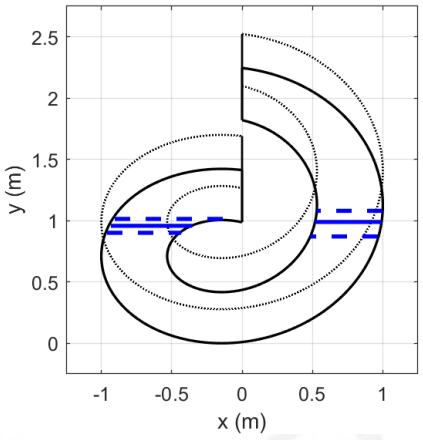


Figure 10. Visualization of water level within one bucket during transit of bucket from inlet to outlet. ($D_o$ = 2 m scale-screw with a surface roughness of $n$ = 0.014.) Observing bucket in the $x$-$y$ plane in the +$z$ direction (cf. Fig. 8). Solid blue lines are mean free-surface level, while dashed blue lines indicate the maximum and minimum levels observed.

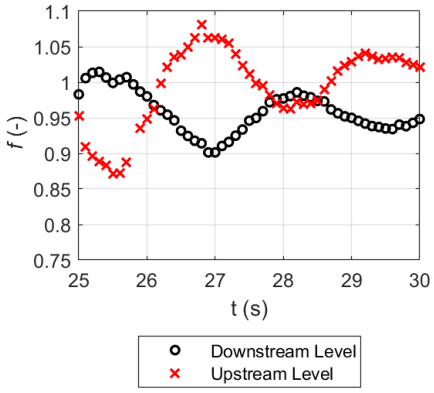


Figure 11. Fill height ratio of the up- and downstream side of the bucket as it traverses the length of the screw. Time is in reference to simulation time; the simulation converged at 19 seconds and this bucket was tracked between 25 and 30 seconds.

periodic static overflow as the water level on the downstream end of the bucket (the high side, i.e. the +x side of Fig. 9 or the left side of Fig. 10) surpassed $z_{max}$ (i.e. $f$ > 1 locally) and instantaneously overflowed. The water level then sloshed back causing a case where local $f$ < 1. This can also be observed in Fig. 10.

Fig. 10 demonstrates the mean, min, and max water levels observed within one bucket during operation. The bucket water level was tracked as it translated along the length of the screw from inlet to outlet. The water level varied significantly after the bucket was formed at the inlet and before it emptied at the outlet of the screw. This suggested that static overflow can occur when the screw operates in regimes that should not induce static overflow (i.e. when $f \leq 1$) if no sloshing was observed.

The sloshing phenomenon was induced at the inlet of the screw as can be seen in Fig. 11. Water rushed into the bucket from the up- to downstream side of the bucket; the dynamic rush of water caused a higher water level on the downstream end of the bucket at first. Once the bucket was fully formed (closed off from the inlet), water no longer entered from the inlet – it then rushed back towards the upstream end of the bucket. The backrush of water caused a higher water level at the downstream end of the bucket. This process carried on, and presumably dampened as the bucket translated through the screw. It then emptied at the outlet of the screw. Interestingly, as surface roughness increased, overflow leakage decreased and became negative (Fig. 12). The negative component of overflow leakage is associated directly with dynamic overflow leakage.

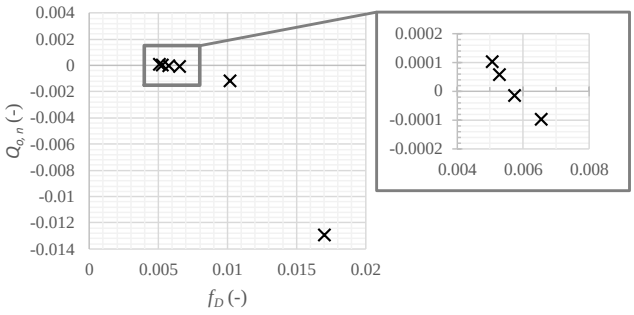


Figure 12. Dimensionless overflow leakage with respect to dimensionless surface roughness.

It seemed that the periodic overflowing was minimized since the rougher walls caused greater wall shear stress and higher frictional effects. In fact, as the roughness increased, cases of negative overflow occurred – water was drawn back up from a downstream bucket along a chute to the previous upstream bucket. Fig. 12 demonstrates the significant impact that surface roughness had on static and dynamic overflow leakage. It seems that rougher walls might have dampened the sloshing effect that caused periodic static overflow and increased the formation of thin films on the blades and inner cylinder associated with dynamic overflow leakage (or friction-leakage).

This phenomenon was observed in operating screw plants, including at Buckfast Abbey (Fig. 2a) and at Romney Weir, Windsor, UK (Fig. 2b). Thin films of water can be observed on the screw blades in both images. Fig. 2a also displays the varying bucket water levels that were observed in the CFD simulations. Qualitatively, it seems that a very large amount of water was drawn up the blades at the Romney Weir (Fig. 2b). The operator of the installation noticed that periodically the screw surfaces get covered by significant algal growth, which would increase blade surface roughness. The operator noted that when the blades were cleaned and the algae was removed, an 11% increase in power production was measured [6]. Similar power increases were noticed at other sites after cleaning and removing algae from the blades and inner cylinder [44], suggesting that the combined effects of friction losses and dynamic overflow leakage were very significant.

Frictional losses have been accounted for in the literature [20], [26], however, overflow is currently only modelled statically [26], [29]. The CFD simulations described in this article will be used for further development of screw performance models by adding capabilities to account for screw rotation speed and thin film development on the blades and inner cylinder.

## IV. Conclusion

Frictional losses and overflow leakage in an Archimedes screw were shown to be significantly impacted by changes to screw surface roughness. Overflow leakage transitioned from positive (flowing into the downstream bucket of the chute) to negative values (flowing back into the upstream bucket of the chute) as roughness increased for a screw operating at an average bucket fill ratio of $f = 1$. Positive overflow is associated with static, water-level-based overflow. Conversely, negative overflow is associated with dynamic overflow leakage through friction-based thin-films. Therefore, the change from positive to negative overflow indicated that dynamic overflow leakage was more dominant than static overflow leakage when surface roughness values were $n \geq 0.012$ (corresponding to smooth steel or rougher) for this specific set of simulations. The authors suggest that most ASGs have blade roughness values corresponding to painted steel ($n = 0.014$) or higher, depending on levels of algal growth and fouling. Significant dynamic overflow leakage was observed in real-world screws, suggesting dynamic overflow leakage is a common phenomenon, and additional modelling is required to account for it in current performance prediction models. Further research will focus on using the data and analyses from this study to aide in model development so overflow leakage (including both static and dynamic modes) may be predicted more accurately. Accurate performance predictions allow designers to optimize screw plant design to make powerplants more economically efficient.


## Acknowledgment

This work is part of larger long-term research program that has been financially supported by the Natural Science and Engineering Research Council (NSERC) of Canada, Collaborative Research and Development (CRD) program (grants CRDPJ 433740-12 and CRDPJ 513923-17) and Greenbug Energy Inc. (Delhi, Ontario, Canada). The authors gratefully acknowledge the efforts of Tony Bouk and Brian Weber of GreenBug Energy Inc. (Canada) for their continued support. The support of David Mann and Adrian Clayton of Mann Power Consulting Ltd. (UK), Chris Elliot of On Stream Energy Ltd. (UK), David DeChambeau of Southeast Power Engineering Ltd. (UK), Mike Ford of Esk Energy (Yorkshire) Ltd. (UK), Mohamed A. Samaha of RIT Dubai (UAE), and Nicola Fergnani of HydroSmart Srl (Italy) has been invaluable to this research and greatly appreciated.


## References


[1] J. Adlard, “Archimedes’ screw: Copley Hydropower Generator,” Future Energy Yorkshire, Yorkshire, 2011.

[2] Renewables First, “How much does a hydropower system cost to operate?,” *renewablesfirst.co.uk*, 2015. [Online]. Available: https://www.renewablesfirst.co.uk/hydropower/hydropower-learning-centre/how-much-does-a-hydropower-system-cost-to-operate/. [Accessed: 11-May-2020].

[3] Spaans Babcock Hydro Power, “Archimedean Screw Turbine.” Spaans Babcock Hydro Power, Balk, 2012.

[4] O. M. Dada, I. A. Daniyan, and O. . Adaranola, “Optimal Design of Micro Hydro Turbine (Archimedes Screw Turbine) in Arinta Waterfall in Ekiti State, Nigeria,” vol. 4, no. 2, pp. 34–38, 2014.

[5] D. Bennion, “Maintaining Archimedes Screw Pumps,” *ECS Engineering Services*, 2013. [Online]. Available: http://www.ecsengineeringservices.com/maintaining-archimedes-screw-pumps/. [Accessed: 10-Oct-2019].

[6] D. Dechambeau, “Personal Communication with David Dechambeau.” Southeast Power Engineering Ltd, Windsor, England, 2019.

[7] D. Kumar and S. S. Katoch, “Environmental sustainability of run of the river hydropower projects: A study from western Himalayan region of India,” *Renew. Energy*, vol. 93, pp. 599–607, 2016.

[8] C. D. McNabb, C. R. Liston, and S. M. Borthwick, “Passage of Juvenile Chinook Salmon and other Fish Species through Archimedes Lifts and a Hidrostal Pump at Red Bluff, California,” *Trans. Am. Fish. Soc.*, vol. 132, no. 1985, pp. 326–334, 2003.

[9] P. Kibel, “Archimedes Screw Turbine Fisheries Assessment. Phase II: Eels and Kelts,” Moretonhampstead, Devon, 2008.

[10] A. T. Piper, P. J. Rosewarne, R. M. Wright, and P. S. Kemp, “The impact of an Archimedes screw hydropower turbine on fi sh migration in a lowland river,” *Ecol. Eng.*, vol. 118, no. March 2018, pp. 31–42, 2018.

[11] P. Kibel and T. Coe, “Fish Monitoring and Live Fish Trials.

Archimedes Screw Turbine, River Dart.," Moretonhampstead, Devon, 2007.

[12] I. S. Pauwels *et al.*, "Multi-Species Assessment of Injury , Mortality , and Physical Conditions during Downstream Passage through a Large Archimedes Hydrodynamic Screw," *Sustainability*, vol. 12, no. 8722, pp. 1–25, 2020.

[13] United Kingdom Environment Agency, "Hydropower Good Practice Guidelines Screening requirements," York, England, 2012.

[14] T. B. Havn *et al.*, "Downstream migration of Atlantic salmon smolts past a low head hydropower station equippped with Archimedes screw and Francis turbines," *Ecol. Eng.*, vol. 105, pp. 262–275, 2017.

[15] L. Sumino Co., "Renewable energy: Micro Hydraulic Power Unit (Spiral Type Pico-Hydro Unit 'PicoPica10', 'PicoPica500')," *United Nations Industrial Development Organization: Investment and Technology Promotion Office, Tokyo*, 2019. [Online]. Available: http://www.unido.or.jp/en/technology_db/5276/. [Accessed: 15-Jan-2021].

[16] Renewables First, "Case study: Archimedes screw turbine at Buckfast Abbey," *Renewables First*, 2012. [Online]. Available: https://www.renewablesfirst.co.uk/project-blog/archimedes-screw-turbine-buckfast-abbey/. [Accessed: 15-Jan-2021].

[17] Landustrie Sneek BV, "Hydropower: Linton Lock (UK)," *Landustrie.nl*, 2017. [Online]. Available: https://www.landustrie.nl/en/products/hydropower/projects/linton-lock.html. [Accessed: 03-Mar-2020].

[18] A. Lashofer, W. Hawle, and B. Pelikan, "State of technology and design guidelines for the Archimedes screw turbine," *Univ. Nat. Resour. Life Sci. Vienna*, no. October, pp. 1–8, 2012.

[19] A. Kozyn, S. Ash, and W. D. Lubitz, "Assessment of Archimedes Screw Power Generation Potential in Ontario CCTC 2015 Paper Number 1570095585," no. 1570095585, pp. 1–11, 2015.

[20] A. Kozyn and W. D. Lubitz, "A power loss model for Archimedes screw generators," *Renew. Energy*, vol. 108, pp. 260–273, 2017.

[21] M. Lyons and W. D. Lubitz, "Archimedes screws for microhydro power generation," in *Proceedings of the ASME 2013 7th International Conference on Energy Sustainability & 11th Fuel Cell Science*, 2013, pp. 1–7.

[22] N. Fergnani and P. Silva, "Archimedean screw and intake head losses : design optimization under variable flows and variable speed," in *Hydro 2016*, 2016.

[23] S. J. Williamson, B. H. Stark, and J. D. Booker, "Low head pico hydro turbine selection using a multi-criteria analysis," *Renew. Energy*, vol. 61, no. 0, pp. 43–50, 2014.

[24] S. C. Simmons and W. D. Lubitz, "Analysis of internal fluid motion in an Archimedes screw using computational fluid mechanics," *J. Hydraul. Res.*, 2020.

[25] D. Nuernbergk, *Wasserkraftschnecken - Berechnung und optimaler Entwurf von archimedischen Schnecken als Wasserkraftmaschine (Hydropower screws - Calculation and Design of Archimedes Screws used in Hydropower)*, 1st ed. Detmold: Verlag Moritz Schäfer, 2012.

[26] D. M. Nuernbergk, *Wasserkraftschnecken - Berechnung und optimaler Entwurf von archimedischen Schnecken als Wasserkraftmaschine (Hydropower screws - Calculation and Design of Archimedes Screws used in Hydropower)*, 2nd ed. Detmold: Verlag Moritz Schäfer, 2020.

[27] W. D. Lubitz, M. Lyons, and S. Simmons, "Performance Model of Archimedes Screw Hydro Turbines with Variable Fill Level," *J. Hydraul. Eng.*, vol. 140, no. 10, pp. 1–11, 2014.

[28] J. Rohmer, D. Knittel, G. Sturtzer, D. Flieller, and J. Renaud, "Modeling and experimental results of an Archimedes screw turbine," *Renew. Energy*, vol. 94, pp. 136–146, 2016.

[29] K. J. Songin and W. D. Lubitz, "Measurement of fill level and effects of overflow in power-generating Archimedes screws," *J. Hydraul. Res.*, vol. 57, no. 5, pp. 635–646, 2018.

[30] D. M. Nuernbergk and C. Rorres, "An Analytical Model for the Water Inflow of an Archimedes Screw Used in Hydropower Generation," *J. Hydraul. Eng.*, vol. 139, no. 2, p. 120723125453009, 2012.

[31] D. Aigner, "Überfälle," in *Wasserbauliche Mittelungen – Aktuelle Forschungen im Wasserbau 1993 - 2008*, H. B. Horlacher and K.-U. Graw, Eds. Dresden: Technischen Universität Dresden, 2008, pp. 182–200.

[32] S. Simmons, M. Lyons, G. Dellinger, and W. Lubitz, "Effects of varying inclination angle on Archimedes screw generator power production with constant head," in *Proceedings of The Joint Canadian Society for Mechanical Engineering and CFD Society of Canada International Congress 2019*, 2019.

[33] M. Lyons, "Lab Testing and Modeling of Archimedes Screw Turbines," University of Guelph, 2014.

[34] A. Kozyn, "Power Loss Model for Archimedes Screw Turbines," University of Guelph, 2016.

[35] K. Songin, "Experimental Analysis of Archimedes Screw Turbines," University of Guelph, 2017.

[36] S. Simmons, "A Computational Fluid Dynamic Analysis of Archimedes Screw Generators," University of Guelph, 2018.

[37] N. Fergnani and P. Silva, "Technical and economic assessment of an Archimedean screw with variable speed operation under variable flows," Milan, 2016.

[38] N. Fergnani, P. Silva, and D. Bavera, "Efficiency assessment of a commercial size Archimedean screw turbine based on experimental data," in *Hydro 2017*, 2017.

[39] A. Passamonti, "Investigation of energy losses in laboratory and full-scale Archimedes screw generators," Politechnico di Milano, 2017.

[40] H. G. Weller, G. Tabor, H. Jasak, and C. Fureby, "A tensorial approach to computational continuum mechanics using object-oriented techniques," *Comput. Phys.*, vol. 12, no. 620, 1998.

[41] G. Dellinger, P. Garambois, M. Dufresne, A. Terfous, J. Vazquez, and A. Ghenaim, "Numerical and experimental study of an Archimedean Screw Generator," *28th AHR Symp. Hydraul. Mach. Syst. Grenoble, July 4-8*, vol. 2, pp. 1419–1428, 2016.

[42] G. Dellinger *et al.*, "Computational fluid dynamics modeling for the design of Archimedes Screw Generator," *Renew. Energy*, vol. 118, pp. 847–857, 2018.

[43] S. Simmons, G. Dellinger, M. Lyons, A. Terfous, A. Ghenaim, and W. D. Lubitz, "Effects of Inclination Angle on Archimedes Screw Generator Power Production with Constant Head," *J. Hydraul. Eng.*, vol. 147, no. 3, pp. 1–12, 2021.

[44] D. Mann, "Personal Communiation with David Mann." Mannpower, York, England, 2019.